ISIJ International, Vol. 37 (1997), No. 10, pp. 967–976

Conversion of Hematite to Iron Carbides by Gas Phase Carbidization

Alberto N. CONEJO and Gerard P. MARTINS[1)]

Instituto Tecnológico de Morelia, Metallurgy and Mechanics Department, Av. Tecnológico #1500, Col. Lomas de Santiaguito, Morelia, Michoacán 58120, México. 1) Colorado School of Mines, Metallurgical and Materials Engineering Department, Golden, Colorado 80401, USA.

(*Received on December 9, 1996; accepted in final form on June 23, 1997*)

The intrinsic conversion rates of hematite (Fe_2O_3) to carbide (primarily cementite) with a CO–H_2 feed-gas have been measured in the temperature range 550 to 650°C, by employing a micro-thermogravimetric system. As a preliminary analysis phase stability diagrams were developed in a triangular representation to overcome limitations of binary-type diagrams already available in the open literature. In general the reaction sequence was identified as consisting of a high-rate conversion of Fe_2O_3 to Fe (33–75%·min^{-1}) followed by conversion of Fe to Fe_3C. Two stages of carbidization were identified. For the first stage, the conversion rates were higher, from 55 to 75%·min^{-1}, depending on the reactor temperature. The rate of carbidization in the second stage region was lower, in the range of 25 to 35%·min^{-1}. The rate of carbidization was found to increase as temperature decreases, within the range from 600 to 640°C. A model based on adsorption kinetics was developed which qualitatively describes the behavior observed. After conversion of Fe to Fe_3C carbon deposition (sooting) was evident. The catalytic role of cementite (in contrast to Fe) in the heterogeneous sooting-reaction has also been addressed.

KEY WORDS: iron carbide; carbides; carburization; carbidization; kinetics; thermogravimetry; iron oxides.

1. Introduction

Iron carbide feedstock offers the potential for the development of new steel-making technologies for the next millennium. It is, perhaps, a metallurgical product whose time has finally arrived. In 1953, Stelling[1)] disclosed a patent related to the production of iron carbide from particulate iron oxides. More recently, Stephens[2)] (1992) has patented, for a similar system, the production of iron carbide employing a make-up gas comprised of H_2–CH_4. Additionally, a thermodynamic analysis was reported by Hager *et al.*,[3)] (1994), who delineated the phase fields for the Fe–C–O–H system. In conjunction with this information, operating conditions for the production of iron carbide were claimed. The work reported in this paper includes a brief review of a detailed thermodynamic analysis which was conducted[4)] so as to address the limitations of previous such analyses. In addition a kinetic study on the conversion of iron oxides into iron carbides is also presented.

2. Phase Stability Diagrams

Two types of diagrams were developed. A binary representation, whose general features are identical to that reported by Hager *et al.*[3)] and a ternary representation so as to avoid technical limitations of the former.

The computational strategy employed in the development of the phase-stability diagrams was adapted from Ojebuoboh and Martins.[5)] In **Fig. 1**, the stability fields for the Fe–C–O system at 800°K (527°C), is displayed. Only cementite was considered in developing the diagrams displayed in this figure based on previous studies conducted by Hofer,[6)] 1950, who found Hägg carbide to be unstable above 300°C. The figure displays the existence of the iron carbide field in a region where the carbon activities are higher than unity, indicating the potential for carbon deposition. This system possesses three degrees of freedom which are set by specifying temperature, oxygen activity and carbon activity. Con-

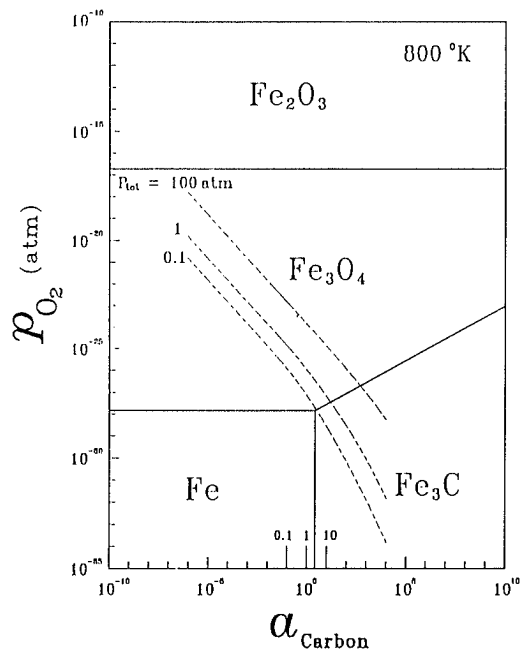

Fig. 1. Phase stability diagram for the system Fe–C–O at 527°C.

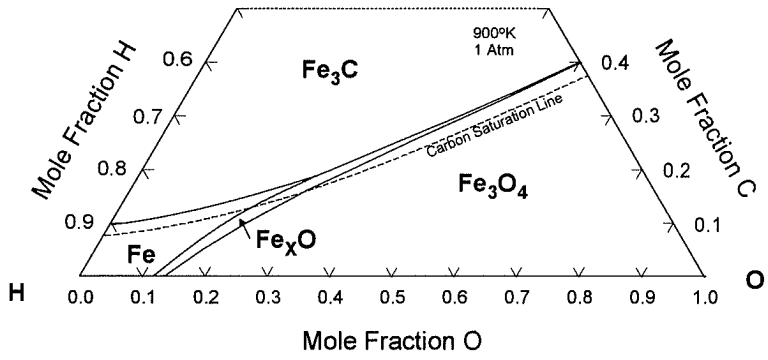

Fig. 2.
Phase stability diagram for the system Fe–C–O–H at 1 atm and 900 K. (627°C, stable configuration)

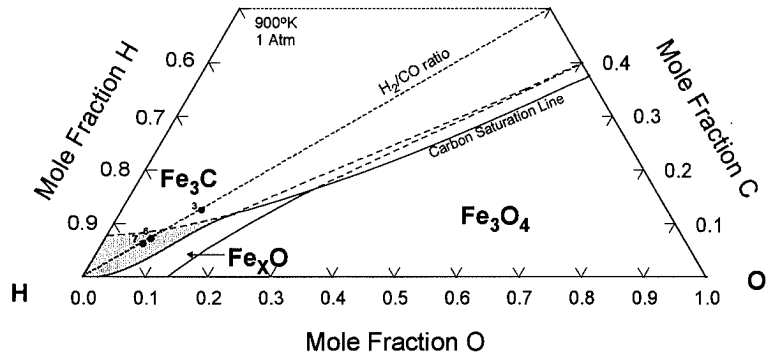

Fig. 3.
Phase stability diagram for the system Fe–C–O–H at 1 atm and 900 K. (627°C, metastable configuration)

sequently, the system total pressure cannot be specified. In contrast, the system total pressure can be specified for the Fe–C–O–H system, since with an additional component included, the degrees of freedom are increased by one, to four. Consequently, the binary representation cannot illustrate directly the effect of the system total-pressure. To overcome this limitation a ternary representation was developed. The ternary phase-stability diagrams representing the formation of iron carbides at isobaric and isothermal conditions are displayed in **Figs. 2** and **3**. Figure 2, (the stable configuration) illustrates that there is the potential for sooting due to the existence of the iron carbide field in the region of carbon supersaturation. Impetus to examine metastable configurations of the condensed phases was prompted by preliminary experiments which had been conducted. These experiments were performed at approximately 627°C (900 K) in a tubular reactor. The reactant gas-mixture was selected based on the information provided by the metastable Fe–C–O–H ternary diagram, this mixture had a H_2/CO ratio of 5 which corresponds to conditions of carbon undersaturation, therefore, if equilibrium is achieved carbon deposition would not be expected. During the experiments, a weight decrease of 25% was observed and attributed to the conversion of hematite to iron carbides. Further chemical analysis by XRD and Mössbauer spectrometry indicated the presence of 100% iron carbides (Fe_3C and Fe_5C_2). These preliminary experiments were successful in the application of the ternary Fe–C–O–H ternary diagrams to select the reactant gas-mixture. The metastable configuration is displayed in Fig. 3. The shaded region in this figure corresponds to the region where iron carbide can be produced without carbon deposition at a given total pressure. Additional experiments employing a thermogravimetric system were conducted subsequently. The results are reported in the following section.

3. Kinetics of Carbidization

Transfer of "carbon" from the gas-phase into the solid is associated with three primary steps: transport of the gas to the reaction interface, surface "reaction", and diffusion into the solid. Carburizing heat-treatment and the manufacture of catalysts employed for the Fischer–Tropsch Synthesis (FTS) of hydrocarbons are two industrial processes, where the process fundamentals on the mechanisms of carburization of iron at high temperatures (900–1 000°C) and the formation of iron carbides at low temperatures (200–400°C), respectively, have been investigated in the past in great detail. This information base is valuable for elucidating the mechanisms associated with the conversion of iron oxides to iron carbides at temperatures between 500 and 700°C.

It would appear, that the precise nature of the phases that contribute to an activated FTS catalyst is still at present, an unresolved issue. It has been widely confirmed that iron oxides do not promote the dissociation of CO (Olmer,[7] 1942). However, whether iron or iron carbide serves as the active phase is highly controversial. Several investigators[8–10] have reported that only metallic iron is the active phase for decomposition of carbon monoxide and that the formation of iron carbides is responsible for the deactivation of iron catalysts. Another group of investigators, contend that iron carbides are active catalysts for the dissociation of CO (Dwyer,[11] 1984; Kock *et al.*,[12] 1985). The techniques employed by those who propose the carbide model appear to be more sophisticated, and modern surface analytical techniques such as low-energy electron diffraction (LEED) have been

employed.

Several authors (Araki and Ponec,[13] 1976; Satterfield,[14] 1991) have proposed a general model for carburization, at conditions employed for synthesis of hydrocarbons (FTS), *i.e.*, temperatures lower than 400°C. In general, the dissociation of the reactant gas on unreacted iron catalysts is proposed to occur in the following manner:

(i) CO is adsorbed and is then dissociated on the catalyst according to the following reactions:

$$\alpha Fe_{(s)} + CO_{(g)} \rightleftharpoons \alpha Fe_{(s)} + CO_{(ad)} \quad \text{.....(1)}$$

$$\alpha Fe_{(s)} + CO_{(ad)} \rightleftharpoons \alpha Fe_{(s)} - \underline{C} + \alpha Fe_{(s)} - O_{(ad)} \quad \text{.....(2)}$$

(ii) Since oxygen has not been detected on the surface, this indicates that it is rapidly desorbed and removed as CO_2 or H_2O, according to:

$$\alpha Fe_{(s)} - O_{(ad)} + CO_{(g)} \rightleftharpoons \alpha Fe_{(s)} + CO_{2(g)} \quad \text{.....(3)}$$

$$\alpha Fe_{(s)} - O_{(ad)} + H_{2(g)} \rightleftharpoons \alpha Fe_{(s)} + H_2O_{(g)} \quad \text{.....(4)}$$

Reactions (1) through (4), can be recast to a more convenient form as:

$$CO_{(g)} + \square \rightleftharpoons CO_{(ad)} \quad \text{.....(5)}$$

$$CO_{(ad)} \rightleftharpoons \underline{C} + O_{(ad)} \quad \text{.....(6)}$$

$$O_{(ad)} + CO_{(g)} \rightleftharpoons CO_{2(g)} + \square \quad \text{.....(7)}$$

$$O_{(ad)} + H_{2(g)} \rightleftharpoons H_2O_{(g)} + \square \quad \text{.....(8)}$$

where $\square \equiv$ vacant interstitial site where surface adsorption takes place.

When methane is also present, the corresponding dissociation reaction is:

$$CH_{4(g)} + \square \rightleftharpoons CH_{4(ad)} \quad \text{.....(9)}$$

$$CH_{4(ad)} \rightleftharpoons \underline{C} + 2H_{2(g)} + \square \quad \text{.....(10)}$$

The effect of hydrogen on carbon-deposition behavior can be discerned by considering Reactions (6) and (8). Hydrogen can consume the adsorbed oxygen on the surface, thus, enhancing the rate of dissociation of CO. It has also been indicated that H_2 increases the rate of adsorption of CO (interactive co-adsorption). Kolesnik and St. Pierre[9] (1980) hypothesized this phenomenon to the existence of an activated complex, (COH)*, but did not provide experimental confirmation. In the experiments conducted, they observed that an increase in H_2O partial-pressure, increased the rate of carbon deposition. This behavior agrees with results from Turkdogan *et al.*[10] (1974), in addition he also observed an increase in carbon deposition-rate up to 70% H_2, above this concentration, an increase in $\%H_2$ caused the opposite effect.

Hydrogen enhances carbon deposition and consequently it provides conditions for supersaturation of carbon on the surface. However, it can also decrease the degree of supersaturation, *via* a hydrogenation reaction:

$$\underline{C} + 2H_{2(g)} \rightleftharpoons CH_{4(g)} \quad \text{.....(11)}$$

Taylor[15] (1956) investigated the decomposition of carbon monoxide on iron-bearing catalysts. He delineated certain conditions which promote carbide formation on the basis that iron carbides are formed at high levels of carbon supersaturation, in contrast to low levels when graphite is formed. Thus, carbide formation would be promoted by a high rate of adsorption of carbon atoms, in conjunction with low nucleation-and-growth rates of graphite crystals. The higher mass density of cementite relative to graphite was also cited as another condition which leads to preferential nucleation of iron carbide crystals, rather than the less dense graphite.

Another possible mechanism which can lead to methanation, is the decomposition of iron carbide (Hägg carbide) above 350°C, into graphite and iron atoms. The carbon atoms at the surface then would become available for hydrogenation.

Grabke[16,17] (1970, 1977), conducted detailed investigations on carburization of iron by CH_4–H_2, H_2–CO and CO–CO_2 gas-mixtures. The rate mechanisms for CO–CO_2 mixtures were formulated based on the elementary steps indicated by Reactions (6)and (7):

$$CO_{(ad)} \underset{k_1^-}{\overset{k_1^+}{\rightleftharpoons}} \underline{C} + O_{(ad)}; \quad \frac{k_1^+}{k_1^-} = K_1 \quad \text{.....(12)}$$

$$CO_{(g)} + O_{(ad)} \underset{k_2^-}{\overset{k_2^+}{\rightleftharpoons}} CO_{2(g)} + \square; \quad \frac{k_2^+}{k_2^-} = K_2 \quad \text{.....(13)}$$

Grabke, in his experiments with CO–CO_2 gas-mixtures observed that the rate-determining step was due to formation/decomposition of CO_2. The forward and reverse rate-equations, for carbon formation in a constant volume system, could then be written as:

Forward Rate:

$$V\frac{d^fC}{dt} = A(1-\theta_o)k_2^+ p_{CO}\cdot O_{(ad)} = A(1-\theta_o)k_2^+ K_1 \frac{p_{CO}^2}{a_C} \quad \text{.....(14)}$$

on the basis that Reaction (12) is at (or close to) equilibrium (equilibrium constant, K_1).

Reverse Rate:

$$V\frac{d^rC}{dt} = -A(1-\theta_o)k_2^- p_{CO_2} \quad \text{.....(15)}$$

The overall rate equation is therefore:

$$V\frac{dC}{dt} = A(1-\theta_o)\cdot\left(k_2^+ K_1 \frac{p_{CO}^2}{a_C} - k_2^- p_{CO_2}\right); \quad [\equiv]\ \text{mol}\cdot\text{min}^{-1} \quad \text{.....(16)}$$

When the parameters are lumped together, then this becomes:

$$r_c = k_f \frac{p_{CO}^2}{a_C} - k_r p_{CO_2} \quad \text{.....(17)}$$

On introducing the equilibrium carbon activity, a_C^{eq}, in terms of the partial pressures of CO and CO_2, Eq. (16) becomes:

$$r_c = k' p_{CO_2}\left(\frac{a_C^{eq}}{a_C} - 1\right); \quad [\equiv]\ \text{mol}\cdot\text{min}^{-1} \quad \text{.....(17')}$$

where: $\frac{d^f}{dt}, \frac{d^r}{dt}$ ≡ forward and reverse rates, respectively.

$k_f[\equiv]$ mol·cm^{-2}·min^{-1}·atm^{-2}

$k_r[\equiv]$ mol·cm^{-2}·min^{-1}·atm^{-1}

A ≡ surface area of Fe

$(1-\theta_0)$ ≡ fraction of the surface not-covered by adsorbed oxygen

r_C ≡ rate of carbidization.

There is disagreement on the controlling reaction when hydrogen is present in the gas mixture. Grabke[16] (1977), had attributed the controlling reaction to the dissociation of CO. More recently, Kaspersma and Shay[18] (1981) identified the reaction involving the dissociation of H_2O (Reaction (8)), rather than the reaction involving the dissociation of CO_2 or CO, as the rate limiting reaction. The dissociation reaction for CO was discarded by these authors who cited experiments by Kishi and Roberts, on the intrinsic rate of CO dissociation on iron films as higher than that of H_2, at temperatures as low as 70°C. The rates of the forward and reverse reactions which remove the adsorbed oxygen, are then based on the reaction:

$$H_{2(g)} + O_{(ad)} \underset{k_3^-}{\overset{k_3^+}{\rightleftharpoons}} H_2O_{(g)} + \square\ ; \quad \frac{k_3^+}{k_3^-} = K_3 \quad ...(18)$$

Forward Reaction:

$$V\frac{dC_C^f}{dt} = A(1-\theta_o)k_3^+ p_{H_2}\cdot O_{(ad)} = A(1-\theta_o)k_3^+ K_1 \frac{p_{H_2}p_{CO}}{a_C} \quad .....(19)$$

Reverse Reaction:

$$V\frac{dC_C^r}{dt} = -A(1-\theta_o)k_3^- p_{H_2O} \quad .....(20)$$

The overall reaction is therefore:

$$V\frac{dC_C}{dt} = A(1-\theta_o)\cdot\left(k_3^+ K_1 \frac{p_{H_2}p_{CO}}{a_C} - k_3^- p_{H_2O}\right);$$

$$[\equiv] \text{mol}\cdot\text{min}^{-1}$$

Neither Grabke nor Kaspersma and Shay, considered solid-state diffusion of carbon to be a significant rate-determining step for carburization.

4. Experimental

Measurement of reaction rates associated with the conversion of iron oxide (hematite) to iron carbides was conducted using a thermogravimetric analysis (TG/DTA) system. Hematite (reagent grade) was chosen as the precursor solid reactant on the basis that it has been demonstrated to have higher reduction rates compared to magnetite-type iron ores. Its chemical composition is indicated in **Table 1**. The powder consisted of particle sizes including clusters, in the range of 0.2 to 0.4 micrometer. The carbidizing gas-mixture was composed of hydrogen and carbon monoxide.

Table 1. Chemical composition of hematite.

Component	wt%
Fe_2O_3	99.4
Insoluble in HCl	0.15
Phosphate (PO_4)	0.01
Sulfate (SO_4)	0.16
Copper (Cu)	0.002
Manganese (Mn)	0.04
Zinc (Zn)	0.002

The TG/DTA system employed was a SEIKO unit (SSC 5200H). Calibration of flowmeters was conducted using a soap-film flowmeter. Phase analyses of the solid product were conducted by X-ray diffraction analysis (XRD) and by Mössbauer spectrometry. The Mössbauer was a Wissel system. The sample must exhibit nuclear resonance; iron being a classical example. Each iron compound has a unique resonance spectrum due to characteristic interactions of the Fe nucleus with its local electronic, magnetic and structural environment. A radioactive source (typically 50 mCi ^{57}Co in Rh) is employed. An oscillatory motion is imparted to the source. Detection of the γ-rays, absorbed resonantly by the ^{57}Fe atoms in the sample, is accomplished with an in line γ-ray counter. A spectrum of transmitted γ-rays *versus* Doppler velocity is thus generated.

Surface area analyses were conducted using an automated gas sorption analyzer, manufactured by Coulter Instruments (Model Omnisorp-100). Data obtained are used to calculate the surface area, based on the B.E.T. adsorption isotherm. Densities of the solid products were measured with a pycnometer, with *n*-tetradecane ($nC_{14}H_{30}$) as the displacement liquid, which provided for complete wetting of the sample, as the displacement liquid.

A forecast of the expected weight changes during the conversion process was determined based on the original mass of the starting solid precursor. If the end-product is Fe_3O_4, FeO, Fe, Fe_3C or Fe_5C_2, the weight decrease is (mass %); 3, 10, 30, 25 and 24 respectively.

Preliminary experiments allowed characteristics of the conversion process to be identified. Depending on the concentration of hydrogen in the gas-mixture and the reactor-temperature, it was possible to control the conditions such that either complete or incomplete reduction occurred before carbidization started. Conditions of gas-phase composition and temperature which allowed for complete reduction (±1%) were chosen so that interpretation of reaction rates would be simple. The actual mechanisms leading to carbidization when incomplete reduction precedes the weight gain (and associated carbidization) cannot be analyzed in a simple manner. It is possible that the rate of carbidization exceeds the rate of reduction and therefore carbidization is initiated without complete reduction to metallic iron. If the reaction of carbidization starts before complete reduction is achieved, intrinsic rates of carbidization cannot be determined explicitly (that is, it is not possible to define the degree of conversion to iron carbide at the minimum point on the curve). For this reason, the experiments selected for kinetic analysis were those where complete reduction was attained and subsequently, the analysis for carbidization could be made on the basis of conver-

sion of metallic iron into iron carbides. This strategy would then allow the intrinsic kinetics of the conversion of Fe to iron carbides to be determined. In addition, the process of carbidization, for temperatures and Y_{H_2}/Y_{CO} ratios (mole fraction of hydrogen to mole fraction of carbon monoxide ratios) leading to complete reduction, can be associated unambiguously with the formation of metallic iron as the exclusive precursor. This scheme allowed the process to be separated into two parts, namely, reduction and carbidization.

The experimental conditions for temperature were selected based on a thermodynamic assessment. According to the analysis, for operation at ambient pressure, the reactor-temperatures should lie in the range 550–650°C (based on a make-up gas comprised of C–H). For a selected temperature, the gas composition was determined from the H_2/CO tie-line of the C–H–O ternary diagram. The procedure employed to conduct the series of experiments consisted of the introduction of the reactant gas mixture when isothermal conditions prevailed in the TGA/reactor-tube (argon was employed for preheating to the desired temperature). The total flow-rate of reactant gas mixture was 400 SCCM (higher flow rates impeded the achievement of isothermal conditions). The mass of hematite employed was approximately 20 mg.

5. Results and Discussion

5.1. Reduction with H_2–CO Mixtures

The rates of reduction reported correspond to the last stage of reduction (80–95% conversion), a region that exhibited a constant rate of reduction. It was observed that the rates of reduction for CO–H_2 mixtures were higher than that for Ar–H_2 mixtures. The results interpreted by an Arrhenius-type analysis are shown in **Fig. 4** for two different Y_{H_2}/Y_{CO} ratios (3 and 6). The apparent activation energy for CO–H_2 mixtures was 30 kJ·mol^{-1}. This activation energy, for reduction with CO–H_2 mixtures, is an indication of a mixed-control mechanism, where both gas diffusion and chemical reaction influence the reaction rate.

5.2. Carbidization of Iron Oxides with H_2–CO Gas-mixtures

The general profile of reduction/carbidization displayed in **Fig. 5** shows two experiments, one conducted at a carbidization temperature of 590°C and the other at 620°C. Both temperatures are above the critical temperature for the formation of wüstite. The corresponding sample temperature profiles are also displayed in the same figure. The response displayed is percent of original mass *versus* elapsed time, results from the introduction of a reactant gas mixture with a ratio $Y_{H_2}/Y_{CO}=6$. It takes less than one minute for the reactant mixture to reach the reaction zone where the sample-pan is located. Rapid reduction of Fe_2O_3 to Fe_3O_4 takes place in approximately 30 sec. Two additional slopes before complete reduction is achieved can be observed, and the change in rate of reduction occurs for a decrease in mass of approximately 10%. This change is associated with the conversion of magnetite to wüstite. The final rate of reduction can therefore be correlated with the conversion of wüstite to metallic iron. The total time for reduction is approximately 4 min, and 50 to 60% of this time is required to effect the last stage of reduction, confirming previous reports (Edström,[19] 1953; Turkdogan,[20] 1980) that the conversion of $Fe_xO \rightarrow Fe$ is the slowest reduction step leading to iron. After reduction is completed (or is close to being completed), the solid undergoes a weight gain associated with carbidization. Two distinct rates of

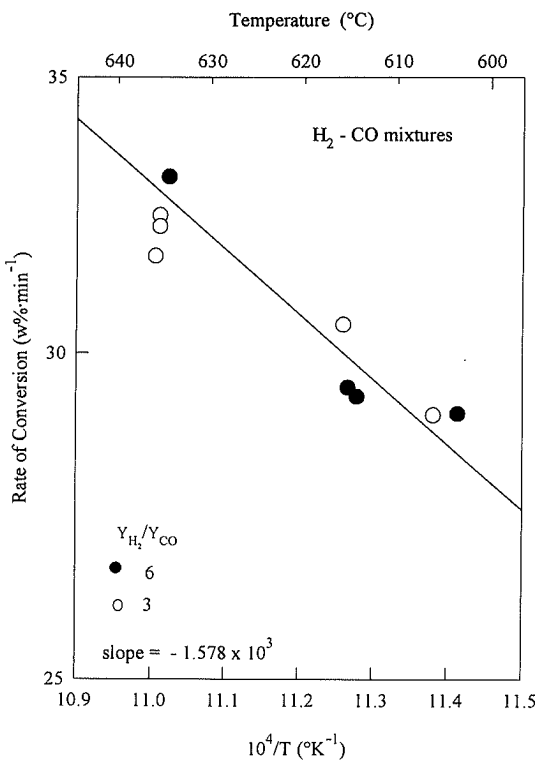

Fig. 4. Arrhenius analysis for the reduction of iron oxides with CO–H_2.

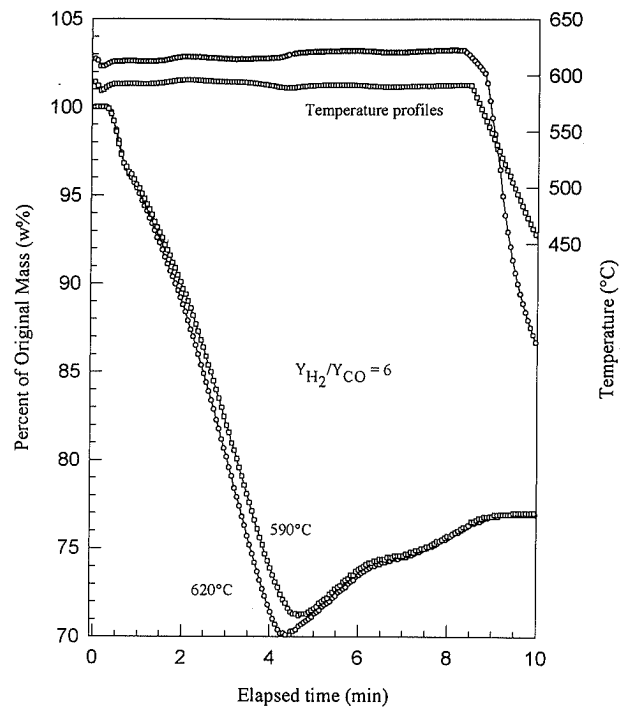

Fig. 5. Overall profile for reduction and carbidization with CO–H_2.

reaction occur during carbidization.

Previous investigations[7-9] have reported the presence of metallic iron as a condition for precipitation of free carbon. In this research, free carbon was always formed after complete conversion of metallic iron to iron carbide. Thus, it provides experimental evidence that iron carbides can serve as a catalyst for the decomposition of carbon monoxide. In the past, it has been suggested that iron carbide cannot promote the formation of free carbon, due to some evidence of cessation of carbon precipitation at the onset of formation of iron carbides. While it is not possible to exclude the possibility that iron carbides may inhibit carbon precipitation under specific conditions, it is evident for H_2–CO mixtures with ratios from 3 to 7 and temperatures from 600 to 640°C, that the active catalyst for carbon deposition is in fact iron carbide.

Figures 6 and **7** show the carbidization behavior for two Y_{H_2}/Y_{CO} ratios, as a function of temperature. The reduction stages are not presented in these figures in order to focus on carbidization. There are three major characteristics that can be observed from these results:

- Anomalous higher rates as temperature decreases,
- Two different rates of reaction (two slopes) within the region of conversion from metallic iron to cementite, and,
- An approximately well defined degree of conversion associated with the change of slopes.

The rate of carbidization increased with a decrease in temperature. This behavior indicated that the carbidization process is complex and involved the interaction of more than one mechanistic step.

Two asymptotic time-independent reaction rates were observed during carbidization. The time associated with the first stage was approximately one minute. The transition to the second stage could also be related with a certain degree of conversion (100% conversion—Fe_3C). The transition to the second stage occurred at a conversion of 70–75%, where a decrease in rate occurred to the second asymptotic value. This phnomenon was initially attributed to the possible formation of an intermediate carbide (Fe_4C) prior to the final conversion to Fe_3C. However, a detailed analysis by Mössbauer spectrometry conducted on samples quenched in both the first-stage and second-stage regions did not corroborate this contention. Stated previously, Mössbauer spectrometry exploits a highly sensitive nuclear γ-ray resonance phenomenon. The spectra are acquired with the aid of an oscillating γ-ray radioactive source. Each iron compound yields a unique spectrum which is used to identify and quantify the phases present.

Figure 8 shows the Mössbauer results for two Y_{H_2}/Y_{CO} ratios, for samples quenched before the complete conversion to cementite (θ-carbide). It is seen that the Mössbauer spectra are associated exclusively with the formation of only one type of iron carbide; in addition, the presence of small amounts of unconverted metallic iron (6 and 7%) is evident. Some metallic iron was expected because the sample had been quenched slightly prior to the start of the second stage. **Figure 9** shows the results for samples quenched in the second stage region,

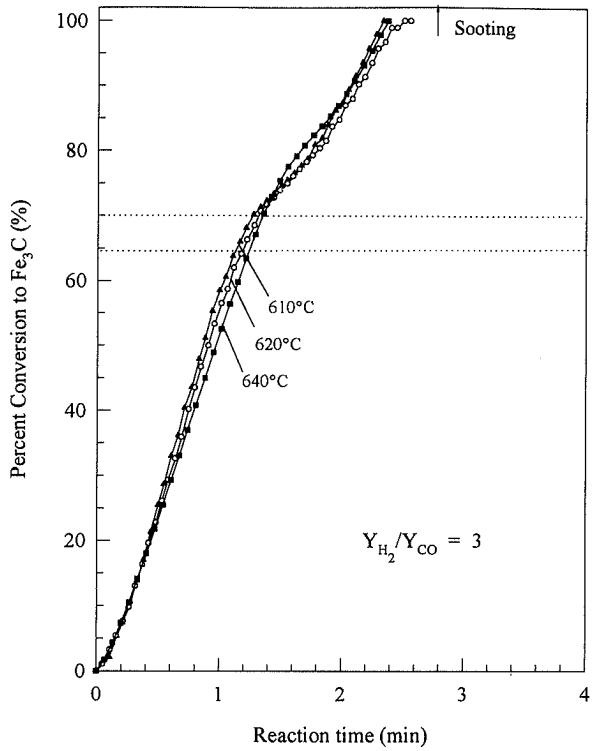

Fig. 6. Percent conversion of Fe to Fe_3C. $Y_{H_2}/Y_{CO}=3$.

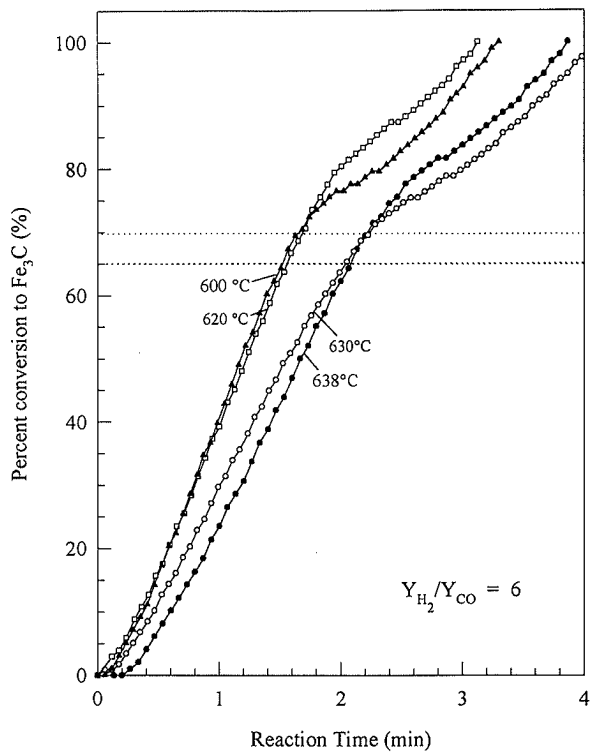

Fig. 7. Percent conversion of Fe to Fe_3C. $Y_{H_2}/Y_{CO}=6$.

which corresponded to the expected formation of θ-carbide. The product is comprised, as in the previous case, primarily of θ-carbide with smaller amounts of unconverted metallic iron (1 and 3%). It was found that the lowest amount of metallic iron corresponded to the sample that employed the larger concentration of carbidizing gas (lower Y_{H_2}/Y_{CO} ratio). It is now apparent that the change in reaction rate behavior is most likely related to structural changes which occur progressively

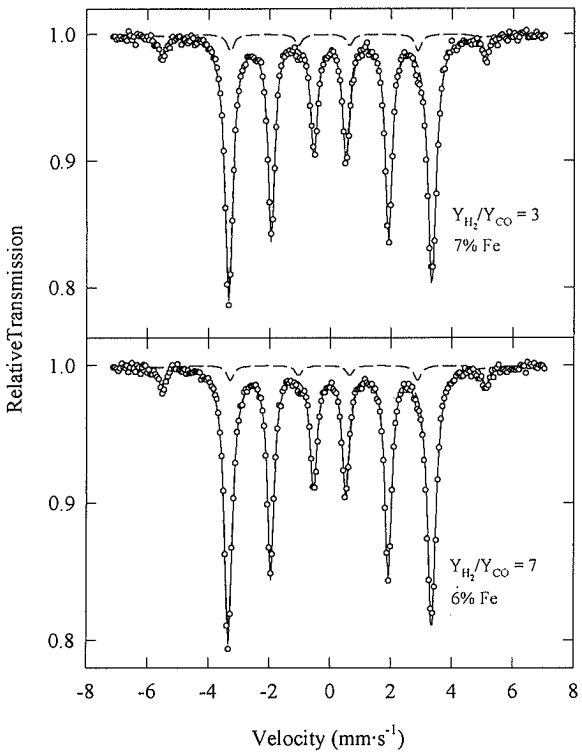

Fig. 8. Mössbauer analysis for quenched samples. Initial carbidization stage. (a) $Y_{H_2}/Y_{CO}=3$, (b) $Y_{H_2}/Y_{CO}=7$. Transmission normalized by dividing by the off resonance count. % Fe represents unconverted metallic iron.

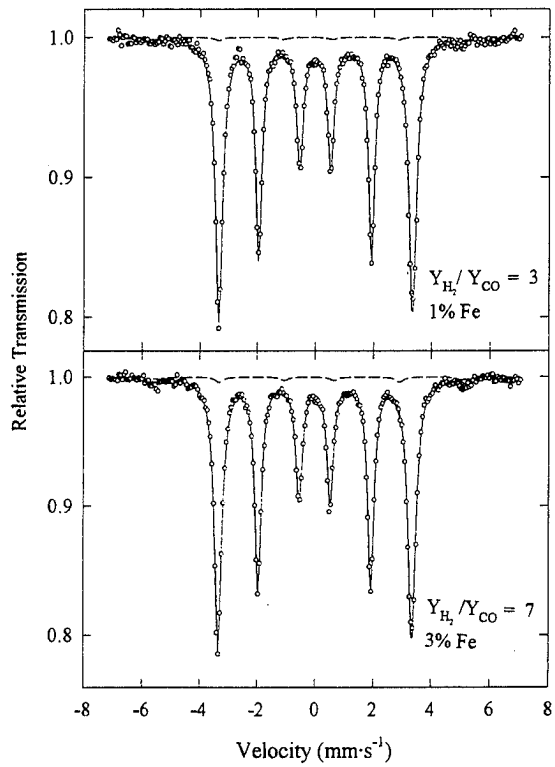

Fig. 9. Mössbauer analysis for quenched samples. Second (final) carbidization stage. (a) $Y_{H_2}/Y_{CO}=3$, (b) $Y_{H_2}/Y_{CO}=7$. (% Fe) represents unconverted metallic iron.

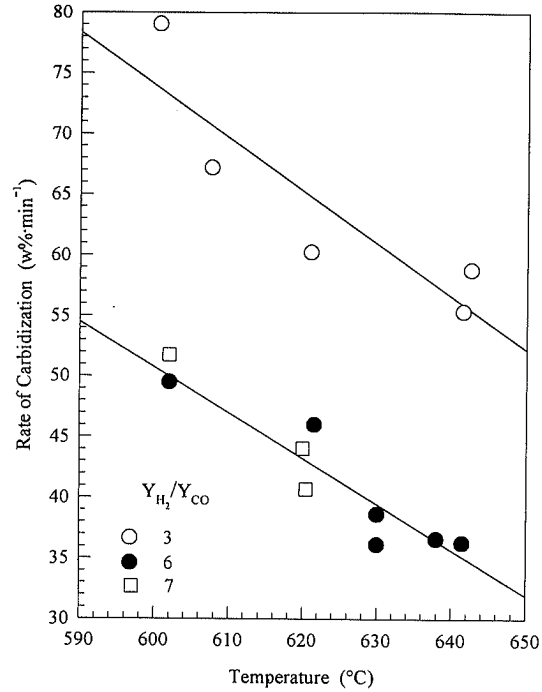

Fig. 10. Rates of carbidization as a function of temperature. Initial stage of carbidization. $Y_{H_2}/Y_{CO}=3$, 6, and 7.

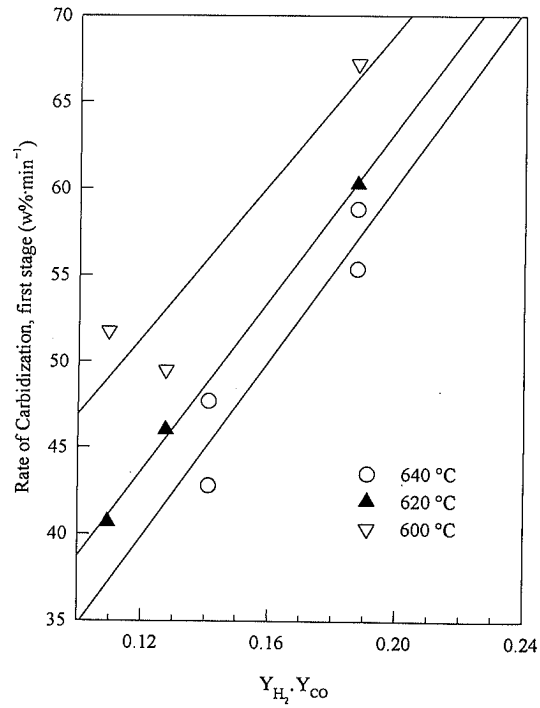

Fig. 11. Effect of the product $Y_{H_2}\cdot Y_{CO}$ on the rate of carbidization at several temperatures.

during the conversion from Fe. The results obtained, based on quenching the reaction at a pre-determined weight change, highlight the importance of using the weight change as a parameter to identify the degree of conversion.

Figure 10 is another representation of the carbidization rate as a function of temperature. In this figure the results for three ratios (3, 6 and 7) are presented. The scatter in the data was attributed to fluctuations in temperature during the stage of carbidization and also due to minor

fluctuations in the flow rate. These results also indicate higher rates of reaction when the concentration of the carbidizing gas (CO) was increased. It was also evident that the difference in the rates of reaction between two gas compositions containing low concentration of carbidizing gas (Y_{H_2}/Y_{CO} ratios of 6 and 7), was not appreciable. More precisely, the rate of carbidization was found to be dependent on the quantity Y_{H_2}/Y_{CO} rather than a sole dependency on the mole-fraction of CO. This correlation, for the first-stage of carbidization, is displayed in **Fig. 11**, for three selected temperatures. This behavior was subsequently reviewed based on a rate-model developed.

Morphological characterization was conducted by SEM for samples quenched before and after the change in rates of carbidization. The morphology of both structures appeared to be similar. This feature was also observed in experiments conducted employing metallic iron as a precursor. If the original morphology of the precursor is globular, the product will remain globular. Thus, it can be concluded that the morphology of iron carbide depends upon the original morphology of the solid reactant.

Experiments conducted with metallic iron as a precursor showed, in principle, similar behavior to those where the iron oxide was first reduced to metallic iron. This result indicates that a requirement for carbidization is the presence of metallic iron.

Based on these experimental results, it was possible to formulate a mechanism of carbidization, applying principles of adsorption kinetics. Previous investigations[21,22] on carbidization have assigned adsorption as the rate limiting mechanism. The fact that the rates of carbidization increased with a decrease in temperature, within the temperature range investigated (590–640°C), was anomalous but not unexpected in chemical kinetics. To explain the results of the present investigation, it is postulated that two reactions primarily control the overall process:

$$Fe_{(s)}+CO_{(g)}+\square \underset{k_2}{\overset{k_1}{\rightleftharpoons}} Fe_{(s)}+CO_{(ad)} \quad \text{.....(21)}$$

$$H_{2(g)}+CO_{(ad)} \overset{k_3}{\rightharpoonup} H_2O_{(g)}+C_{(s)}+\square \quad \text{.....(22)}$$

$$3Fe_{(s)}+C_{(s)} \overset{k_4}{\rightharpoonup} Fe_3C_{(s)}\,; \quad k_4 \gg k_3 \quad \text{.....(23)}$$

Several other mechanisms might be used to interpret the rates observed, such as the dissociation of CO on the surface producing adsorbed carbon and adsorbed oxygen, where oxygen is subsequently desorbed by hydrogen. Another scenario could incorporate the adsorption reaction of hydrogen on the surface, which could then react with oxygen adsorbed; *etc.* The mechanism portrayed by Reactions (21) and (22) appears to be a simple one, which in fact describes the rates observed. It consists of reversible adsorption of one species, carbon monoxide and subsequently irreversible dissociation of the adsorbed CO on the iron surface by hydrogen present in the gas-phase. Adsorption of hydrogen is not considered due to the presence of carbon monoxide.[23] The mechanism proposed includes reaction between an adsorbed species [$CO_{(ad)}$] and a gas species (H_2), this mechanism is referred to as a Rideal mechanism (Laidler,[24] 1954).

Based on the scheme proposed, Reaction (22) defines the rate of production of carbon atoms on the iron surface. According to this reaction, the rate of formation of carbon atoms is equal to the rate of desorption of $CO_{(ad)}$, which depends on the fraction coverage of CO molecules on the surface (θ_1):

$$r''_{Fe_3C}=r_C=r_{CO_{(d)}}=k_3 p_{H_2}\theta_1 \quad \text{.....(24)}$$

where: θ_1 = fraction coverage of carbon monoxide.

The overall rate of adsorption of CO, on the basis of a steady state approximation, is approximately zero. Thus, Reactions (21) and (22) define this overall rate. According to Reaction (21) the rate of adsorption is proportional to the fraction of sites available for $CO_{(ad)}$ and to the partial pressure of hydrogen, in the reverse direction. The rate of desorption is proportional to the fraction of sites occupied by $CO_{(d)}$:

$$k_1 p_1(1-\theta_1)-k_2\theta_1-k_3 p_2\theta_1=0 \quad \text{.....(25)}$$

where: $1 \equiv CO_{(ad)}$
$2 \equiv H_{2(g)}$.

The general solution for the fraction coverage of CO (θ_1), is obtained by solving Eq. (24). Recasting this equation, the following expression is obtained:

$$k_1 p_1-(k_1 p_1+k_2+k_3 p_2)\theta_1=0 \quad \text{.....(26)}$$

From which:

$$\theta_1=\frac{k_1 p_1}{k_1 p_1+k_2+k_3 p_2} \quad \text{.....(27)}$$

Then, the heterogeneous rate of formation of iron carbide, r''_{Fe_3C}, is given by the following equation:

$$r''_{Fe_3C}=\frac{k_1 k_3 p_1 p_2}{k_1 p_1+k_2+k_3 p_2} \quad \text{.....(28)}$$

To visualize the behavior exhibited by this equation, it is necessary to define the values for the rate constants, as well as the magnitude of the partial pressures. This was conducted using values reported in the literature. Gadsby *et al.*[25] (1948) reported the rate constants for the rate of adsorption of CO, in terms of an Arrhenius expression, as follows:

$$K=\frac{k_1}{k_2}=10^{-8}e^{(+45\,500\pm 3\,500/RT)}\,\text{atm}^{-1}$$

Using this reference, a proper selection for k_1 and k_2, was chosen, such that the behavior observed could be predicted by the rate equation, within the temperature region of interest. The value for k_3 was determined by successive approximations, in accordance with the same criterion. It should be stated that the magnitude of the rate constants only serve to validate the rate equation proposed. However, the experimental results obtained can only provide semi-quantitative information on the rate expression that describes the formation of iron

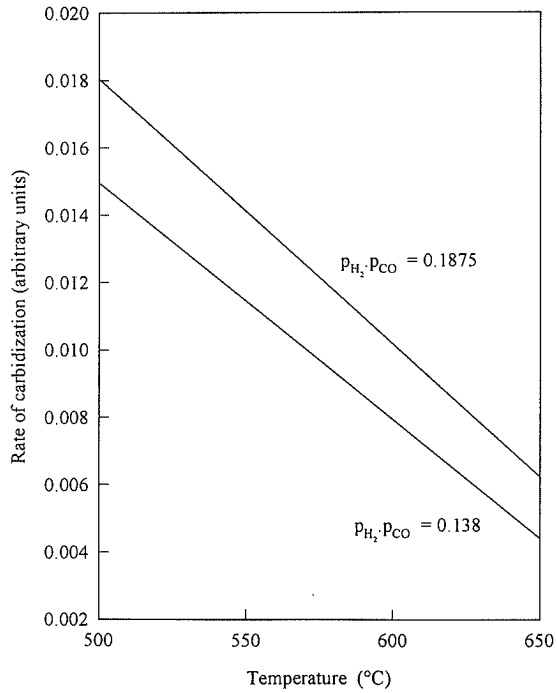

Fig. 12. Rate of carbidization as a function of temperature based on the proposed model.

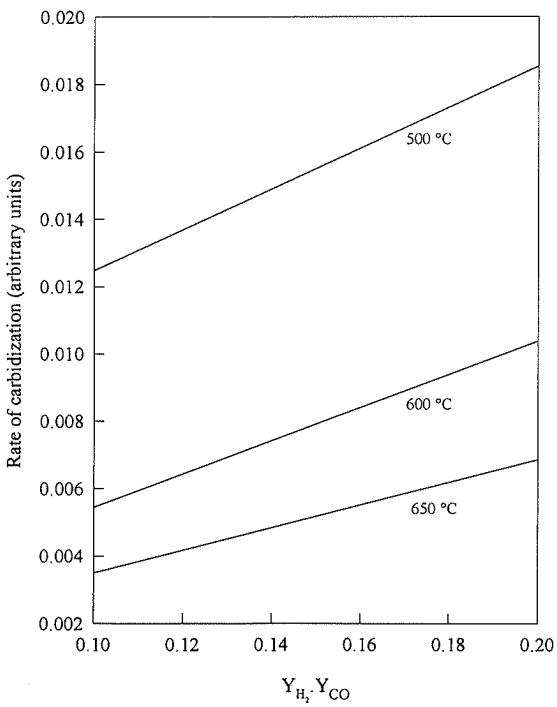

Fig. 13. Model predictions of the effect of the product $Y_{H_2} \cdot Y_{CO}$ on the rate of carbidization, at several temperatures.

carbides.

The results are displayed in **Figs. 12** and **13**. Figure 12 displays the rate of carbidization as a function of temperature. It can thus be concluded that the rate equation proposed predicts an increase in the rate of carbidization as temperature decreases. This behavior cannot be explained in a simple manner based on the rate equation proposed, but is in fact due to the presence of hydrogen in the system. Figure 13 shows the effect of the product of partial pressures of CO and H_2,

Table 2. Surface area measurements.

Material	A_{sp} ($m^2 \cdot g^{-1}$)	V_m ($ml \cdot g^{-1}$)
Fe_2O_3	7.18	1.6502
Fe_3C (10% Fe)	2.04	0.4687
Fe_3C (6% Fe)	2.54	0.5841

indicating a linear dependency, in agreement with the observed results.

5.3. Large Batch-sample Carbidization

The work conducted with the thermogravimetric system (TGA) employed a sample-size of 15–20 mg (reagent grade ferric oxide). Several experiments were conducted in a tubular reactor in order to evaluate the behavior of a larger sample-size and also to obtain enough material for surface area and density analysis. Reagent-grade hematite and CO–H_2 mixtures were employed. The sample size employed was from 1 000 to 1 300 mg. The conversion process from iron oxides to iron carbides was determined by the total mass change.

The reactor temperature was approximately 620°C. Two Y_{H_2}/Y_{CO} ratios were evaluated, 3 and 7, corresponding to saturated and undersaturated conditions. The reactor total pressure was the ambient pressure in Golden, approximately 0.8 atm. Since carbidizing gas is not required for reduction, this stage was conducted under a flow of hydrogen at $1\,l \cdot min^{-1}$.

The carbide product was then analyzed by SEM, Mössbauer Spectrometry, and its surface area and density were measured. The final weight changes in all cases produced a total mass change of 25%. The Mössbauer analysis identified cementite as the primary constituent with some traces of unconverted metallic iron (6–10%).

The results from surface area analysis are presented in **Table 2**. Three samples were analyzed: commercial hematite and the solid products from the experiments conducted in the tubular reactor. It was found that the B.E.T. equation could predict the experimental results between 0.001 to 0.03 units of the relative pressure. It is observed that the conversion of iron oxides to iron carbides involves a decrease in the specific surfae area, by a factor of 3. This may be an attractive feature in regard to the potential oxidation of the carbide phase.

The results from density measurements, of the iron carbide products (cementite), at 24°C, ranged from 7.63 to $7.72\,g \cdot ml^{-1}$; a magnitude intermediate between iron oxides and metallic iron. Lange's Handbook cites a values of $7.69\,g \cdot ml^{-1}$ at room temperature. Density corrections due to the small (6 to 10%) presence of iron was not considered. It appears that because of the slight differences in densities between cementite and metallic iron, the measured values were in good agreement with the published value.

6. Conclusion

The following enumerated conclusions represent the contributions of this research to the knowledge-base on conversion kinetics of iron oxides into iron carbide by gas-phase carbidization:

(1) For the H_2–CO feed-gas mixtures (which most probably have not been fully equilibrated), the conversion process of iron oxides into iron carbides progresses through the following sequence (at temperatures where wüstite is stable):

$$Fe_2O_{3(s)} \rightarrow Fe_3O_{4(s)} \rightarrow Fe_xO_{(s)} \rightarrow Fe^{\circ}_{(s)} \rightarrow Fe_3C_{(s)}$$

However, the intermediates Fe_3O_4 and Fe_xO were not identified by phase analysis but rather by gravimetric response in the TGA-system.

(2) a) The reduction of $Fe_2O_3 \rightarrow Fe_3O_4$ exhibits the highest rate in the pre-reduction sequence. In agreement with previous studies on reduction of iron oxides, the rate of reduction was increased with either an increase in temperature or hydrogen partial pressure, when reduction was conducted with hydrogen. The apparent activation energy for reduction of iron-oxides with H_2–CO mixtures was found to be 30 kJ/mol. This value, according to the interpretation advanced by previous investigators, is an indication of a reduction process where the roles of both chemical reaction and diffusion are significant in determining the overall rate of reduction.

b) Between 600–640°C, two stages of carbidization were identified, for the conditions inherent to the H_2–CO feed-gas mixtures and the TGA reactor system employed in this research. In the first stage, the reaction rate is approximately invariant for up to 70–75% conversion (based on Fe). The corresponding conversion rates were 55 to 75 mass%/min for a Y_{H_2}/Y_{CO} ratio of 3 and corresponding temperatures in the range 640 to 600°C. The rate of carbidization in the second region is lower and for the temperature range 640 to 590°C the corresponding measured conversion rates were 25–35 mass%/min for a Y_{H_2}/Y_{CO} ratio of 3.

c) For the feed-gas compositions employed, and acknowledging that this gas is (most probably) not equilibrated in the TGA-reactor tube (absence of significant concentrations of CH_4, CO_2 and H_2O relative to the equilibrium values), the first stage carbidization rate was found to decrease with increasing temperature. This is a manifestation of the interaction between CO and H_2 in the carbidization mechanism as described by the proposed reaction-model (Eq. (24)). At a fixed temperature this rate can be correlated by the product of the feed-gas mole fractions $Y_{H_2} \cdot Y_{CO}$.

d) The increased rate of carbidization at lower temperatures, 600 or 590°C relative to 640°C has been semi-quantitatively demonstrated by a reaction-rate model. The proposed mechanism consists of the adsorption of CO onto a pre-reduced iron surface, coupled to the dissociation of adsorbed CO and subsequent scavenging of oxygen from the surface by hydrogen in the gas-phase.

(3) There was no appreciable change in morphology of the iron particles obtained in the pre-reduction of the reagent grade Fe_2O_3 during its conversion of $Fe^{\circ} \rightarrow Fe_3C$.

(4) The cementite produced from the reagent grade hematite used in this research had a specific surface area of 2.0 to 2.5 $m^2 g^{-1}$, which is 70% smaller than that of the precursor. Its density (of the product Fe_3O+6 to 10% Fe) was found be: $7.68 \pm 0.04\ g \cdot m/^{-1}$.

Acknowledgements

The authors are grateful to Professor Don Williamson of the Physics Department at Colorado School of Mines (CSM)–USA, for providing assistance with the Mössbauer analyses. One of the authors (ACN) gratefully acknowledges the financial support from the Mexican Government (through the National Council for Science and Technology—CONACYT) to complete PhD studies at CSM, and a leave of absence provided by Instituto Tecnologico de Morelia.

REFERENCES

1) O. Stelling: USA Patent 2780 537, (1957).
2) F. M. Stephens, Jr.: USA Patent 5137 566, (1992).
3) J. P. Hager, F. A. Stephens and F. M. Stephens, Jr.: USA Patent 5366 897, (1994).
4) A. N. Conejo: Ph. D. Thesis, Colorado School of Mines, (1995).
5) K. F. Ojebuoboh: PhD Thesis, Colorado School of Mines, (1985).
6) L. J. E. Hofer: *Catalysis*, **4** (1956), 373.
7) F. Olmer: *J. Phys. Chem.*, **46** (1942), 405.
8) N. F. Kolesnik and G. R. St. Pierre: *Metall. Trans.*, **11B** (1980), 285.
9) M. P. Manning and R. C. Reid: *Ind. Eng. Chem. Process Des. Dev.*, **16** (1977), 358.
10) E. T. Turkdogan and R. G. Olsson: *Metall. Trans.*, **5** (1974), 21.
11) D. J. Dwyer and J. H. Hardenbergh: *J. Catalysis*, **87** (1984), 66.
12) A. J. H. M. Kock, P. K. De Bokx, E. Boellaard, W. Klop and J. W. Geus: *J. Catalysis*, **96** (1985), 468.
13) M. Araki and V. Ponec: *J. Catalysis*, **44** (1976), 439.
14) Ch. N. Satterfield: Heterogeneous Catalysis in Industrial Practice, 2nd Ed., MacGraw Hill, New York, (1991).
15) J. Taylor: *J. Iron Steel Inst.*, (1956), 1.
16) H. J. Grabke: *Metall. Trans.*, **1** (1970), 2927.
17) H. J. Grabke: *Ann. Rev. Mater. Sci.*, **5** (1977), 155.
18) J. H. Kaspersma and R. H. Shay: *Metall. Trans.*, **12B** (1981), 77.
19) J. O. Edström: *J. Iron Steel Inst.*, (1953), 289.
20) E. T. Turkdogan: Physical Chemistry of High Temperature Technology, Academic Press, New York, (1980), 412.
21) E. T. Turkdogan and J. V. Vinters: *Metall. Trans.*, **5** (1974), 11.
22) M. P. Manning and R. C. Reid: *Ind. Eng. Chem. Process Des. Dev.*, **16** (1977), 358.
23) P. Marcus and J. Oudar: Hydrogen Degradation of Ferrous Alloys, Noyes Publications, New Jersey, (1985), 36.
24) J. K. Laidler: Catalysis, Vol. I, Reinhold Publishing Co., New York, (1954), 75.
25) J. Gadsby, F. J. Long, P. Sleightholm and K. W. Skyes: *Proc. R. Soc. London*, **193A** (1948), 357.